

ON THE USE OF THE VIRTUAL ELEMENT METHOD FOR GEOMECHANICS ON RESERVOIR GRIDS

ODD ANDERSEN, HALVOR M. NILSEN, AND XAVIER RAYNAUD

ABSTRACT. In this paper we study the use of Virtual Element method for geomechanics. Our emphasis is on applications to reservoir simulations. The physical processes that form the reservoirs, such as sedimentation, erosion and faulting, lead to complex geometrical structures. A minimal representation, with respect to the physical parameters of the system, then naturally leads to general polyhedral grids. Numerical methods which can directly handle this representation will be highly favorable, in particular in the setting of advanced work-flows. The Virtual Element method is a promising candidate to solve the linear elasticity equations on such models. In this paper, we investigate some of the limits of the VEM method when used on reservoir models. First, we demonstrate that care must be taken to make the method robust for highly elongated cells, which is common in these applications, and show the importance of calculating forces in terms of traction on the boundary of the elements for elongated distorted cells. Second, we study the effect of triangulations on the surfaces of curved faces, which also naturally occur in subsurface models. We also demonstrate how a more stable regularization term for reservoir application can be derived.

1. INTRODUCTION

Modeling of sedimentary subsurface naturally leads to general unstructured grids due to stratigraphic layering, erosion processes and the presence of faults. The industry standard for reservoir grids is the corner point grids [13]. Many geometrical grid formats have been proposed to improve on this format, for example Skua Grid [8], S-Grid, Faulted S-Grid and Cut-Cell [11], but all compact representation of the underlying geology will lead to cells with high aspect ratio, distorted cells, faces or cells of very different sizes, cells or faces with different shapes. Methods which are robust for different grid types will greatly simplify the modeling of subsurface physics.

In recent years, the coupling of geomechanical effects with subsurface flow has become more and more important in many areas including: oil and gas production from mature fields, oil and gas production from fractured tight reservoirs, fractured rock for geothermal application and risk assessment of CO₂ injection. Realistic modeling of these applications is hampered by the differences in the way geomechanics and flow models are build and discretized. Traditionally, the mechanic problems are solved using finite element methods but they are difficult to adapt to the standard representation of reservoir simulations. In contrast, the Virtual Element Methods (VEM) can operate on general polyhedral grids. As such, the ability of the method to handle irregular grids makes it very attractive for geomechanical applications. In this paper, we investigate if the method can effectively be applied on realistic reservoir grids. Our main result concerns the treatment of the load term. We observe that standard regularization terms used in the literature are not adapted to elongated with large aspect ratios, which are standard in geological models. We propose a modification of the regularization constant which can be used in the 2D case and a dual based approach to compute the load term which turns out to be little sensitive to the choice of regularization and can be easily extended to 3D. In a first part of this paper, we present the VEM method following mostly [7] but we also tried to clarify the connection with the construction of the projection operators as given in the basic principles of [3]. In our numerical experiments, we will focus on the performance of the VEM method on geological grids. The emphasis will be on corner point grids and complex small scale sedimentary models. To be able to demonstrate the VEM method in the reservoir setting we used the MRST framework [10] to simplify the grid handling.

2. THE EQUATIONS OF LINEAR ELASTICITY

We consider the equation of linear elasticity for small deformations. The displacement is given by $\mathbf{u}(\mathbf{x}) \in \mathbb{R}^d$ for $d = 2, 3$ (2D or 3D case) and $\mathbf{x} \in \Omega \subset \mathbb{R}^d$. The equations are given by

$$(1) \quad \nabla \cdot \boldsymbol{\sigma} = \mathbf{F}$$

with

$$(2) \quad \boldsymbol{\sigma} = \mathbf{C}\boldsymbol{\varepsilon} \quad \text{and} \quad \boldsymbol{\varepsilon} = \frac{1}{2}(\nabla + \nabla^T)\mathbf{u}$$

Here, $\boldsymbol{\sigma}$, $\boldsymbol{\varepsilon}$ and \mathbf{u} denote the Cauchy stress tensor, the infinitesimal strain tensors and the displacement field, respectively. The vector \mathbf{f} is an external volumetric force. The linear operator \mathbf{C} is a fourth order stiffness tensor which satisfies, for

some constant $c > 0$, the ellipticity condition

$$(3) \quad c \mathbf{S} : \mathbf{S} \leq \mathbf{S} : \mathbf{C} \mathbf{S},$$

for any symmetric matrix $\mathbf{S} \in \mathbb{R}^{d \times d}$. The symbol $:$ denotes the scalar product in $\mathbb{R}^{d \times d}$ defined as

$$(4) \quad \mathbf{A} : \mathbf{B} = \text{tr}(\mathbf{A}^T \mathbf{B}),$$

for any $\mathbf{A}, \mathbf{B} \in \mathbb{R}^{d \times d}$.

3. PRESENTATION OF THE VEM METHOD FOR LINEAR ELASTICITY

The VEM method was first introduced in the framework of Mimetic Finite Element methods but later rephrased in the language of finite element methods (see [6] for discussions). A general presentation of VEM is given in [3]. The same authors present convergence results for linear elasticity in [5]. Our implementation of the VEM follows the presentation done in [7]. We rewrite the equation of linear elasticity equation rewritten in the weak form,

$$(5) \quad \int_{\Omega} \boldsymbol{\varepsilon}(\mathbf{v}) : \mathbf{C} \boldsymbol{\varepsilon}(\mathbf{u}) \, dx = \int_{\Omega} \mathbf{f} \cdot \mathbf{v} \, dx,$$

for all displacement \mathbf{v} . We decompose the bilinear form in cell contributions,

$$(6) \quad a(\mathbf{u}, \mathbf{v}) = \int_{\Omega} \boldsymbol{\varepsilon}(\mathbf{u}) : \mathbf{C} \boldsymbol{\varepsilon}(\mathbf{v}) \, dx = \sum_E \int_E \boldsymbol{\varepsilon}(\mathbf{u}) : \mathbf{C} \boldsymbol{\varepsilon}(\mathbf{v}) \, dx = \sum_E a_E(\mathbf{u}, \mathbf{v}),$$

where E spans over the grid cells. In the rest of this presentation, we consider a given cell E and will denote by \mathcal{V}_E the approximating function space in E . In the VEM approach, the basis functions of \mathcal{V}_E are not known explicitly but, for a first-order VEM method, the requirements on \mathcal{V}_E are that it contains the space of polynomials of order 1, denoted $\mathbb{P}_1(E)$, and that the bilinear form $a_E(\mathbf{u}, \mathbf{v})$ can be computed exactly for any $\mathbf{u} \in \mathbb{P}_1(E)$ and any $\mathbf{v} \in \mathcal{V}_E$, using only the degrees of freedom of \mathbf{v} . As in the standard finite element method, the degrees of freedom are the nodal displacements, so that the continuity at the boundaries of each element is ensured by requiring linearity on the edges and a local reconstruction on the faces, which depends only on the values at the edges of the face where the reconstruction is done. The system matrix can be assembled element-wise. Let us denote

$$\mathcal{V}_E^{\text{scalar}} = \{\mathbf{v} \in H^1(E) \mid \mathbf{v}|_e \in \mathbb{P}_1(e) \text{ for all edges } e\},$$

for $i = 1, \dots, d$. For a given node η of E , we can construct a function ϕ_η in $\mathcal{V}_E^{\text{scalar}}$ such that $\phi_\eta(\bar{\eta}) = 1$ if $\bar{\eta} = \eta$ and zero otherwise. The basis virtual functions of \mathcal{V}_E are then given by

$$\phi_\eta^k(\mathbf{x}) = \phi_\eta(\mathbf{x}) \mathbf{e}_k$$

for $\eta \in N(E)$ and $k = 1, \dots, d$, where $N(E)$ denotes the set of nodes of the cell E . After having introduced the projection operator, we will add some extra requirements for ϕ_η concerning the first and second order moment. But beside that, no more explicit properties for ϕ_η are needed and this is one of the important point of the method, which also makes it so flexible.

In the general framework of VEM, as introduced in [3], the computation of the projection operator typically requires the computation of an inverse, locally for each cell. The formulation in [7] has the advantage of giving an explicit expression for

the projection operator. In the presentation that follows, we will try to clarify the connection between the two approaches.

3.1. The kynematics of affine displacement. The physics of linear elasticity is associated with linear deformations, in particular the rigid body motions play a crucial role. Let us recall some simple facts on the kynematics of affine displacements. The linear space of affine displacements, which we denote by \mathcal{P} , corresponds to the sum of the translations and linear transformation so that any $\mathbf{l} \in \mathcal{P}$ can be written as $\mathbf{l}(\mathbf{x}) = \mathbf{u} + \mathbf{L}\mathbf{x}$, for $\mathbf{u} \in \mathbb{R}^d$ and $\mathbf{L} \in \mathbb{R}^{d \times d}$. The dimension of the space of \mathcal{P} is $d^2 + d$. The subspace of rigid body motion, which we denote \mathcal{P}_r , contains the rotation and the translation. Any $\mathbf{l} \in \mathcal{P}_r$ can be written as

$$(7) \quad \mathbf{l}(\mathbf{x}) = \mathbf{u} + \boldsymbol{\Omega}(\mathbf{x} - \mathbf{x}_0),$$

for any \mathbf{u} , $\mathbf{x}_0 \in \mathbb{R}^d$ and $\boldsymbol{\Omega}$ that belongs to the space of skew-symmetric matrices, denoted $\text{aSym}(\mathbb{R}^d)$. The decomposition of an element $\mathbf{l} \in \mathcal{P}_r$ given by (7) is not unique and the space \mathcal{P}_r is isomorphic to the sum of the two spaces given by the space of translation and the space of skew-symmetric matrices. The dimension of \mathcal{P}_r is therefore $d(d+1)/2$. The space of non rigid body motion is the quotient of \mathcal{P} with respect to \mathcal{P}_r , which we denote $\mathcal{P}/\mathcal{P}_r$. We introduce the projection operator $\boldsymbol{\pi}_c$ in \mathcal{P} defined as

$$(8) \quad \boldsymbol{\pi}_c(\mathbf{l}) = \frac{1}{2}(\mathbf{L} + \mathbf{L}^T)(\mathbf{x} - \bar{\mathbf{x}}_E),$$

for any $\mathbf{l}(\mathbf{x}) = \mathbf{u} + \mathbf{L}\mathbf{x} \in \mathcal{P}$. Here, $\bar{\mathbf{x}}_E$ denotes the arithmetic average of the positions \mathbf{x}_i of all the nodes of the cell E , that is

$$\bar{\mathbf{x}}_E = \frac{1}{n} \sum_{i=1}^n \mathbf{x}_i,$$

where n corresponds to the number of nodes in E . We can check that $\boldsymbol{\pi}_c(\mathbf{l}) = 0$ if and only if $\mathbf{l} \in \mathcal{P}_r$. Hence, the image of $\boldsymbol{\pi}_c$ is in bijection with the space of linear strain $\mathcal{P}/\mathcal{P}_r$ which we therefore identify to $\mathcal{P}_c = \boldsymbol{\pi}_c(\mathcal{P})$. Note that \mathcal{P}_c can also be defined as

$$(9) \quad \mathcal{P}_c = \{\mathbf{l} \in \mathcal{P} \mid \nabla \mathbf{l} = \nabla \mathbf{l}^T \text{ and } \mathbf{l}(\bar{\mathbf{x}}_E) = 0\}.$$

Then, we introduce the projection $\boldsymbol{\pi}_r$ from \mathcal{P} to \mathcal{P}_r as,

$$(10) \quad \boldsymbol{\pi}_r(\mathbf{l}) = \mathbf{l} - \boldsymbol{\pi}_c(\mathbf{l}) = \mathbf{l}(\bar{\mathbf{x}}_E) + \frac{1}{2}(\mathbf{L} - \mathbf{L}^T)(\mathbf{x} - \bar{\mathbf{x}}_E).$$

We can check that $\mathcal{P}_r = \boldsymbol{\pi}_r(\mathcal{P})$, $\boldsymbol{\pi}_c \boldsymbol{\pi}_r = \boldsymbol{\pi}_r \boldsymbol{\pi}_c = 0$, $\boldsymbol{\pi}_c + \boldsymbol{\pi}_r = \mathbf{I}_p$. The space \mathcal{P}_c is isomorphic to the space of symmetric matrices, denoted Sym . We consider the case $d = 3$ and use Kelvin's notation to represent Sym so that, for any $\mathbf{a} \in \text{Sym}$, its Kelvin representation in \mathbb{R}^6 , which we denote $\hat{\mathbf{a}} \in \mathbb{R}^6$, is given by

$$(11) \quad \hat{\mathbf{a}}^T = [a_{11}, a_{22}, a_{33}, \sqrt{2}a_{23}, \sqrt{2}a_{13}, \sqrt{2}a_{12}].$$

The square root in the definition above leads to the following correspondence between the scalar products in Sym and \mathbb{R}^6 ,

$$(12) \quad \mathbf{a} : \mathbf{b} = \hat{\mathbf{a}} \cdot \hat{\mathbf{b}},$$

for any $\mathbf{a}, \mathbf{b} \in \text{Sym}$. Note that Kelvin notations are not used in [7]. We define the symmetric tensor $\hat{\mathbf{C}} \in \mathbb{R}^{6 \times 6}$ by the identity

$$(13) \quad \mathbf{a} : \mathbf{C}\mathbf{b} = \hat{\mathbf{a}}^T \hat{\mathbf{C}} \hat{\mathbf{b}},$$

for all $\mathbf{a}, \mathbf{b} \in \text{Sym}$. Then, we obtain that, for any $\mathbf{l}, \mathbf{m} \in \mathcal{P}$, we have

$$(14) \quad a_E(\mathbf{l}, \mathbf{m}) = \int_E \boldsymbol{\varepsilon}(\mathbf{l}) : \mathbf{C} \boldsymbol{\varepsilon}(\mathbf{m}) \, d\mathbf{x} = |E| \widehat{\boldsymbol{\pi}_c(\mathbf{l})}^T \hat{\mathbf{C}} \widehat{\boldsymbol{\pi}_c(\mathbf{m})}$$

The projection $\boldsymbol{\pi}_c(\mathbf{l})$ belongs to \mathcal{P}_c and can therefore be written as $\boldsymbol{\pi}_c(\mathbf{l}) = \mathbf{Q}(\mathbf{x} - \hat{\mathbf{x}}_E)$ for $\mathbf{Q} \in \text{Sym}$. In (14), we wrote $\widehat{\boldsymbol{\pi}_c(\mathbf{l})}$ for the Kelvin representation $\hat{\mathbf{Q}}$ of \mathbf{Q} , and similarly for $\widehat{\boldsymbol{\pi}_c(\mathbf{m})}$. For the space \mathcal{P}_r , we use the mapping between aSym and \mathbb{R}^3 given by the cross-product operation. For any $\mathbf{a} \in \text{aSym}$, we can define a rotation vector $\hat{\mathbf{a}} \in \mathbb{R}^3$ as

$$(15) \quad \hat{\mathbf{a}} = \sqrt{2}[-a_{2,1}, a_{1,2}, -a_{1,2}]^T.$$

Then, we have

$$(16) \quad \mathbf{a}\mathbf{x} = \frac{1}{\sqrt{2}} \hat{\mathbf{a}} \times \mathbf{x}$$

and

$$(17) \quad \mathbf{a} : \mathbf{b} = \hat{\mathbf{a}} \cdot \hat{\mathbf{b}}$$

for any $\mathbf{a}, \mathbf{b} \in \text{aSym}$. The normalization using $\frac{1}{\sqrt{2}}$ in (16) is used in order to get an exact correspondence between the scalar products in aSym and \mathbb{R}^3 . The basis of \mathcal{P}_r is given by the canonical basis of \mathbb{R}^6 , the first three components corresponding to the translation vector while the three last components correspond to a rotation vector.

3.2. The projection operator. The projection operator on the space of affine displacement, with respect to the bilinear form a , plays an essential role in the formulation of a first order VEM method. We follow the notation of [3] and denote this projection by $\boldsymbol{\pi}^\nabla$, even if the bilinear form we consider is not the H^1 semi-norm, which is used as example in [3]. For a given displacement function $\boldsymbol{\nu} \in \mathcal{V}_E$, the projection $\mathbf{p} = \boldsymbol{\pi}^\nabla(\boldsymbol{\nu})$ is given as the unique element $\mathbf{p} \in \mathcal{P}$ which satisfies

$$(18a) \quad a_E(\mathbf{p}, \mathbf{q}) = a_E(\boldsymbol{\nu}, \mathbf{q}),$$

for all $\mathbf{q} \in \mathcal{P}$ and such that

$$(18b) \quad \boldsymbol{\pi}_r \mathbf{p} = \boldsymbol{\pi}_r \boldsymbol{\nu},$$

which means that the projection of \mathbf{p} and $\boldsymbol{\nu}$ on \mathcal{P}_r coincide. The condition (18b) is necessary to determine a unique solution. Indeed, the bilinear form a is degenerate as it is invariant with respect to the space of rigid body motion and the condition (18b) eliminates this undeterminacy by imposing a rigid body motion for \mathbf{p} . It is important to note that the definition of the projection operator is in fact independent of \mathcal{V}_E and could be extended to $[H^1(E)]^3$. However, for \mathcal{V}_E , the projection can be computed exactly, using directly the degrees of freedom and without further integrations. Up to now, we have only introduced $\boldsymbol{\pi}_r$ and $\boldsymbol{\pi}_c$ on \mathcal{P} and we will now extend these definitions to \mathcal{V}_E so that the definition in (18b) makes actually sense. We let the reader check that the new definitions of $\boldsymbol{\pi}_c$ and $\boldsymbol{\pi}_r$ on \mathcal{V}_E , when restricted to \mathcal{P} , coincide with those introduced previously. We define the projection $\boldsymbol{\pi}_r : \mathcal{V}_E \rightarrow \mathcal{P}_r$ as

$$(19) \quad \boldsymbol{\pi}_r(\boldsymbol{\nu}) = \bar{\boldsymbol{\nu}}_E + \frac{1}{2} \langle \nabla \boldsymbol{\nu} - \nabla \boldsymbol{\nu}^T \rangle (\mathbf{x} - \bar{\mathbf{x}}_E),$$

where the bracket denote the cell average, i.e.,

$$\langle \mathbf{w} \rangle = \frac{1}{|E|} \int_E \mathbf{w} \, d\mathbf{x} \quad \text{and} \quad \bar{\boldsymbol{\nu}} = \frac{1}{n} \sum_E \boldsymbol{\nu}_i.$$

We define the projection $\boldsymbol{\pi}_c : \mathcal{V}_E \rightarrow \mathcal{P}_c$ as

$$\boldsymbol{\pi}_c(\boldsymbol{\nu}) = \frac{1}{2} \langle \nabla \boldsymbol{\nu} + \nabla \boldsymbol{\nu}^T \rangle (\mathbf{x} - \bar{\mathbf{x}}_E).$$

In a moment, we are going to check that both projections can be computed directly from the degree of freedoms. First, we use these definitions to compute $\boldsymbol{\pi}^\nabla$. We start by considering a solution $\mathbf{p} = \boldsymbol{\pi}^\nabla(\boldsymbol{\nu})$ to (18) and set $\mathbf{p}_c = \mathbf{p} - \boldsymbol{\pi}_r(\boldsymbol{\nu})$. Then, $\boldsymbol{\pi}_r(\mathbf{p}_c) = 0$ and $\mathbf{p}_c \in \mathcal{P}_c$. The symmetric gradient is zero for any element in \mathcal{P}_r , that is $\varepsilon \circ \boldsymbol{\pi}_r = 0$. We have $\mathbf{p} = \boldsymbol{\pi}_c(\mathbf{p}) + \boldsymbol{\pi}_r(\mathbf{p})$ and a similar decomposition for \mathbf{q} . Hence, $a_E(\mathbf{p}, \mathbf{q}) = a_E(\mathbf{p}_c, \mathbf{q}_c)$ and $a_E(\boldsymbol{\nu}, \mathbf{q}) = a_E(\boldsymbol{\nu}, \mathbf{q}_c)$ so that Equation (18a) becomes

$$(20) \quad a_E(\mathbf{p}_c, \mathbf{q}_c) = a_E(\boldsymbol{\nu}, \mathbf{q}_c).$$

Let us now determine the element \mathbf{p} that satisfies (18) for a given $\boldsymbol{\nu} \in \mathcal{V}_E$. The coercivity of the the form a_E on \mathcal{P}_c follows from the definition of \mathcal{P}_c and the coercivity of the tensor \mathbf{C} , see (3). Therefore, there exists a unique solution $\mathbf{p}_c \in \mathcal{P}_c$ such that (20) holds for all $\mathbf{q}_c \in \mathcal{P}_c$. For any $\mathbf{q}_c \in \mathcal{P}_c$, we have

$$(21) \quad a_E(\mathbf{p}_c, \mathbf{q}_c) = \int_E \nabla \mathbf{p}_c : \mathbf{C} \nabla \mathbf{q}_c \, d\mathbf{x} = |E| \nabla \mathbf{p}_c : \mathbf{C} \nabla \mathbf{q}_c$$

and

$$(22) \quad a_E(\boldsymbol{\nu}, \mathbf{q}_c) = \int_E \frac{1}{2} (\nabla \boldsymbol{\nu} + \nabla \boldsymbol{\nu}^T) : \mathbf{C} \nabla \mathbf{q}_c \, d\mathbf{x} = \left(\frac{1}{2} \int_E (\nabla \boldsymbol{\nu} + \nabla \boldsymbol{\nu}^T) \, d\mathbf{x} \right) : \mathbf{C} \nabla \mathbf{q}_c.$$

Hence, $\nabla \mathbf{p}_c = \frac{1}{2} \int_E (\nabla \boldsymbol{\nu} + \nabla \boldsymbol{\nu}^T) \, d\mathbf{x}$ which implies that \mathbf{p}_c is uniquely defined as $\mathbf{p}_c = \boldsymbol{\pi}_c(\boldsymbol{\nu})$. We can conclude that \mathbf{p} defined as

$$(23) \quad \mathbf{p} = \mathbf{p}_c + \boldsymbol{\pi}_r(\boldsymbol{\nu})$$

is the unique solution to (18). Indeed, $\boldsymbol{\pi}_c(\mathbf{p}) = \mathbf{p}_c$ and $\boldsymbol{\pi}_r(\mathbf{p}) = \boldsymbol{\pi}_r(\boldsymbol{\nu})$ are both uniquely defined by (20) and (18b).

Let us now give more details on the assembly. To do so, we consider a basis function $\boldsymbol{\nu}^i \in \mathcal{V}_E$ for which the only non-zero displacement can only occur at the node i , that is $\boldsymbol{\nu}^i(\mathbf{x}_j) = 0$ if $i \neq j$.

has all degrees of freedom but those corresponding to the node i equal to zero. Such function can be written as write it as

$$\boldsymbol{\nu}^i(\mathbf{x}) = \sum_{j=1}^d \nu_j \phi_i(\mathbf{x}) \mathbf{e}_j,$$

where $\{\mathbf{e}_j\}_{j=1}^d$ is the basis for Cartesian coordinates. We have

$$\langle \nabla \boldsymbol{\nu}^i \rangle = \sum_{j=1}^d \nu_j \mathbf{e}_j \langle \nabla \phi_i \rangle^T,$$

and we have to compute $\mathbf{q}^i = \langle \nabla \phi_i \rangle$. The expression above will simplify to

$$\langle \nabla \boldsymbol{\nu}^i \rangle = \boldsymbol{\nu}^i \mathbf{q}^{iT}.$$

For \mathbf{q}^i , we have

$$(24) \quad \mathbf{q}^i = \int_E \nabla \phi_i \, d\mathbf{x} = \int_{\partial E} \phi_i \mathbf{n} \, d\mathbf{x} = \sum_{f \in F_E} \left(\int_f \phi_i \, d\mathbf{x} \right) \mathbf{n}_f,$$

The integral in (24) can be computed exactly

$$(25) \quad \int_f \phi_i \, d\mathbf{x} = \begin{cases} \frac{|f|}{m} + \frac{1}{2} (\mathbf{n}_{e,i^-} + \mathbf{n}_{e,i^+}) \cdot (\mathbf{x}^f - \bar{\mathbf{x}}^f) & \text{in 3D,} \\ \frac{|f|}{2} & \text{in 2D,} \end{cases}$$

where \mathbf{x}^f is the centroid of the face f and $\bar{\mathbf{x}}^f = \frac{1}{m} \sum_{j=1}^m \mathbf{x}_j^f$.

We denote by $\mathbf{W}_c^i \in \mathbb{R}^{6 \times 3}$ the matrix representation of $\boldsymbol{\pi}_c$ written in the basis of displacement for the node i (that is \mathbb{R}^3) and the basis of \mathcal{P}_c (that is \mathbb{R}^6 using the Kelvin notation). For $l, m = \{1, 2, 3\}$, we have

$$\frac{1}{2} \langle \nabla \boldsymbol{\nu} + \nabla \boldsymbol{\nu}^T \rangle_{l,m} = \frac{1}{2} (\nu_l q_m + \nu_m q_l)$$

so that

$$(\mathbf{W}_c^i)^T = \begin{pmatrix} q_1 & 0 & 0 & 0 & \frac{1}{\sqrt{2}}q_3 & \frac{1}{\sqrt{2}}q_2 \\ 0 & q_2 & 0 & \frac{1}{\sqrt{2}}q_3 & 0 & \frac{1}{\sqrt{2}}q_1 \\ 0 & 0 & q_3 & \frac{1}{\sqrt{2}}q_2 & \frac{1}{\sqrt{2}}q_1 & 0 \end{pmatrix}.$$

We have

$$\frac{1}{2} \langle \nabla \boldsymbol{\nu} - \nabla \boldsymbol{\nu}^T \rangle = \frac{1}{2} (\boldsymbol{\nu}^i \mathbf{q}^{iT} - \mathbf{q}^i \boldsymbol{\nu}^{iT}).$$

Using the general identity $(\mathbf{q}^i \times \boldsymbol{\nu}^i) \times \mathbf{x} = (\mathbf{q}^i \cdot \mathbf{x}) \boldsymbol{\nu}^i - (\boldsymbol{\nu}^i \cdot \mathbf{x}) \mathbf{q}^i$, we get that the \mathbb{R}^3 representation of the matrix in aSym above is given by $\frac{1}{\sqrt{2}}\mathbf{q}^i \times \boldsymbol{\nu}^i$. Hence, the matrix $\mathbf{W}_r^i \in \mathbb{R}^{6 \times 3}$ that represents $\boldsymbol{\pi}_r$ written in the basis of displacement for the node i (that is \mathbb{R}^3) and the basis of \mathcal{P}_r (that is \mathbb{R}^6 for the translation and the rotation vector) is given by

$$(\mathbf{W}_r^i)^T = \begin{pmatrix} \frac{1}{n} & 0 & 0 & 0 & -\frac{1}{\sqrt{2}}q_3 & \frac{1}{\sqrt{2}}q_2 \\ 0 & \frac{1}{n} & 0 & \frac{1}{\sqrt{2}}q_3 & 0 & -\frac{1}{\sqrt{2}}q_1 \\ 0 & 0 & \frac{1}{n} & -\frac{1}{\sqrt{2}}q_2 & \frac{1}{\sqrt{2}}q_1 & 0 \end{pmatrix}.$$

The matrices \mathbf{W}_c from the space of all the degrees of freedom (that is \mathbb{R}^{3n}) to \mathcal{P}_c is obtained by concatenating \mathbf{W}_c^i and similarly for \mathbf{W}_r . To obtain from \mathbf{W}_c and \mathbf{W}_r , the matrix representations of $\boldsymbol{\pi}_c$ and $\boldsymbol{\pi}_r$ in terms of the degrees of freedom only, we have to map \mathcal{P}_c and \mathcal{P}_r to the degrees of freedom. To do so, we introduce the vectors \mathbf{r}_i , for $i = \{1, \dots, n\}$ as

$$\mathbf{r}_i = \mathbf{x}_i - \bar{\mathbf{x}}_E.$$

We define $\mathbf{N}_c^i, \mathbf{N}_r^i \in \mathbb{R}^{3 \times 6}$ as

$$(26) \quad \mathbf{N}_c^i = \begin{pmatrix} r_1 & 0 & 0 & 0 & \frac{1}{\sqrt{2}}r_3 & \frac{1}{\sqrt{2}}r_2 \\ 0 & r_2 & 0 & \frac{1}{\sqrt{2}}r_3 & 0 & \frac{1}{\sqrt{2}}r_1 \\ 0 & 0 & r_3 & \frac{1}{\sqrt{2}}r_2 & \frac{1}{\sqrt{2}}r_1 & 0 \end{pmatrix} \quad \text{and} \quad \mathbf{N}_r^i = \begin{pmatrix} 1 & 0 & 0 & 0 & -\frac{1}{\sqrt{2}}r_3 & \frac{1}{\sqrt{2}}r_2 \\ 0 & 1 & 0 & \frac{1}{\sqrt{2}}r_3 & 0 & -\frac{1}{\sqrt{2}}r_1 \\ 0 & 0 & 1 & -\frac{1}{\sqrt{2}}r_2 & \frac{1}{\sqrt{2}}r_1 & 0 \end{pmatrix}.$$

Then, the matrices $\mathbf{N}_c, \mathbf{N}_r \in \mathbb{R}^{3n \times 6}$ are obtained by concatenating $\mathbf{N}_c^i, \mathbf{N}_r^i$, respectively.

The projection can be then written in terms of the degree of freedom as

$$(27) \quad \mathbf{P}_r = \mathbf{N}_r \mathbf{W}_r \quad \text{and} \quad \mathbf{P}_c = \mathbf{N}_c \mathbf{W}_c$$

and the projection on affine displacement is given by $\mathbf{P} = \mathbf{P}_c + \mathbf{P}_r$. For any $\boldsymbol{\nu}, \boldsymbol{\eta} \in \mathcal{V}_E$, we have that

$$a_E(\boldsymbol{\pi}^\nabla \boldsymbol{\nu}, \boldsymbol{\pi}^\nabla \boldsymbol{\eta}) = |E| \widehat{\boldsymbol{\pi}_c(\boldsymbol{\nu})}^T \widehat{\mathbf{C} \boldsymbol{\pi}_c(\boldsymbol{\eta})} = |E| \boldsymbol{\nu}^T \mathbf{W}_c^T \widehat{\mathbf{C} \mathbf{W}_c} \boldsymbol{\eta},$$

where in the last term, slightly abusing the notations, we denote by $\boldsymbol{\nu}, \boldsymbol{\eta} \in \mathbb{R}^{3n}$ the vector composed of the degrees of freedoms of $\boldsymbol{\nu}, \boldsymbol{\eta} \in \mathcal{V}_E$. Using the same convention, we can write the bilinear form as

$$(28) \quad a_{h,E}(\boldsymbol{\nu}, \boldsymbol{\eta}) = \boldsymbol{\nu}^T \left(|E| \mathbf{W}_c^T \hat{\mathbf{C}} \mathbf{W}_c + (\mathbf{I} - \mathbf{P})^T \mathbf{S} (\mathbf{I} - \mathbf{P}) \right) \boldsymbol{\eta}.$$

We note that the decomposition of the energy in two orthogonal parts, the linear part which ensures consistency and the higher order part which are handled so that stability is preserved, is analog to the decomposition used in [4], even if it was introduced there to introduce some freedom in the choice of the basis functions.

3.3. Implementation of force term. The force term can be calculated in several different ways which are equivalent up to the order of accuracy of the methods. We have investigated several alternatives,

- (1) Integration for each node nodal quadrature i.e node weights,
- (2) Integration for each element quadrature i.e cell node weights,
- (3) Computation based on the duality with grad or equivalently as a gradient of a potential.

Alternative 1 is the choice that naturally follows from the VEM approach. Alternative 2 was argued to be simpler and with similar accuracy in [7]. Alternative 3 arises naturally when the force comes from a coupled poro-elastic model. The two first alternatives are equivalent for constant force vectors and give similar results. We show that the last one has significantly less errors than the others for elongated grid cells. As we are going to see, in contrast to the second alternative, it is also independent on the choice of the virtual basis, which makes it a priori more robust with respect to the cell geometry.

For a given force \mathbf{f} , we consider the work done by the force for a given displacement field,

$$(29) \quad \int_{\Omega} \mathbf{f} \cdot \mathbf{u} \, d\mathbf{x}.$$

This expression defines a linear form on the space of displacement. We denote by \mathcal{V} the global discrete function space of displacement, which is constructed by taking the product of the \mathcal{V}_E for all the cells E of the grid and requiring continuity at the element boundaries. We want to find a discrete linear form on \mathcal{V} that approximates (29). We can equip \mathcal{V} with the standard scalar product in \mathbb{R}^{n_N} , that is $\sum_{\eta} \mathbf{u}_{\eta} \cdot \boldsymbol{\nu}_{\eta}$. Here, n_N denotes the total number of nodes. Any linear form on \mathcal{V} can be represented by an element in \mathcal{V} , using this scalar product. Hence, we end up looking for an element $\hat{\mathbf{f}} \in \mathcal{V}$ such that

$$(30) \quad \int_{\Omega} \mathbf{f} \cdot \mathbf{u} \, d\mathbf{x} \approx \sum_{\eta} \hat{\mathbf{f}}_{\eta} \cdot \mathbf{u}_{\eta}.$$

The element $\hat{\mathbf{f}} \in \mathbb{R}^{N_n}$ can be interpreted as a nodal force. We present several expressions for $\hat{\mathbf{f}}$ corresponding to the three alternatives presented previously. First, we can use weights which are obtained using a first-order quadrature. For a node η , let us denote by $E(\eta)$ the set of cells to which the node η belongs. Using quadrature rules to integrate \mathbf{f} on each cell, we obtain

$$(31) \quad \hat{\mathbf{f}}_{\eta} = \sum_{i \in E(\eta)} w_i^{\eta} \mathbf{f}(\eta),$$

see [7] for the definitions of the weights w_i^η . This corresponds to alternative 1. For alternative 2, let $\mathbf{u}^\eta \in \mathcal{V}$ be a displacement for which the only non-zero degrees of freedom are those corresponding to η . Then, we have

$$\begin{aligned}
\int_{\Omega} \mathbf{f} \cdot \mathbf{u}^\eta \, d\mathbf{x} &= \sum_{i \in E(\eta)} \int_{E_i} \mathbf{f} \cdot \mathbf{u}^\eta \, d\mathbf{x} \\
&\approx \sum_{i \in E(\eta)} \int_{E_i} \boldsymbol{\pi}_i^0(\mathbf{f}) \cdot \mathbf{u}^\eta \, d\mathbf{x} \\
&= \sum_{i \in E(\eta)} \boldsymbol{\pi}_i^0(\mathbf{f}) \cdot \int_{E_i} \mathbf{u}^\eta \, d\mathbf{x} \\
(32) \quad &= \sum_{i \in E(\eta)} \boldsymbol{\pi}_i^0(\mathbf{f}) \cdot \int_{E_i} \boldsymbol{\pi}_i^\nabla(\mathbf{u}^\eta) \, d\mathbf{x}.
\end{aligned}$$

Here, $\boldsymbol{\pi}_i^0$ denotes the L^2 projection in the element E_i . To obtain the last integral, we use that fact that the virtual basis functions can be chosen such that the zero and first moment of a function $\boldsymbol{\nu}$ in \mathcal{V}_E coincide with those of its projection $\boldsymbol{\pi}_i^\nabla \boldsymbol{\nu}$, that is

$$\int_E \mathbf{p} \cdot \boldsymbol{\nu} \, d\mathbf{x} = \int_E \mathbf{p} \cdot \boldsymbol{\pi}_i^\nabla(\boldsymbol{\nu}) \, d\mathbf{x},$$

for any $\mathbf{p} \in \mathbb{P}_1$ and $\boldsymbol{\nu} \in \mathcal{V}_E$. See [1] for more details. The choice of such basis implies that, for an element E , the modes that belong to $\ker \boldsymbol{\pi}^\nabla$, typically higher nonlinear modes, will not be excited directly by the force. From (32), we infer that $\hat{\mathbf{f}}_\eta$ is defined as a linear combination of cell averages of \mathbf{f} ,

$$(33) \quad \hat{\mathbf{f}}_\eta = \sum_{i \in E(\eta)} m_i^\eta \boldsymbol{\pi}_i^0(\mathbf{f})$$

where m_i^η are the weights given

$$m_i^\eta = \mathbf{e}_k \cdot \int_{E_i} \boldsymbol{\pi}_i^\nabla(\boldsymbol{\phi}_k^\eta) \, d\mathbf{x}.$$

Note that the expression on the right above do not depend on k , as the same basis function is used in all directions. Let us now turn to alternative 3. We assume that the force can be written as the gradient of a potential, $\mathbf{f} = \nabla \psi$. We have

$$(34) \quad \int_{\Omega} \mathbf{f} \cdot \mathbf{u} \, d\mathbf{x} = \int_{\Omega} \nabla \psi \cdot \mathbf{u} \, d\mathbf{x} = - \int_{\Omega} \psi \nabla \cdot \mathbf{u} \, d\mathbf{x} + \int_{\partial\Omega} \psi \mathbf{u} \, d\mathbf{x} = - \int_{\Omega} \psi \nabla \cdot \mathbf{u} \, d\mathbf{x}.$$

The boundary integral vanishes because we assume Dirichlet boundary condition, $\mathbf{u} = 0$ for $\mathbf{x} \in \partial\Omega$. In the VEM space, there exists a natural discretization of the divergence operator as an operator from \mathcal{V} to cell-wise constant functions denoted \mathcal{T} which is isomorphic to \mathbb{R}^{N_c} , where N_c denotes the number of cells. Indeed, for any discretized potential $\hat{\psi} \in \mathcal{T}$ and $\boldsymbol{\nu} \in \mathcal{V}$, we have

$$(35) \quad \int_{\Omega} \hat{\psi} \nabla \cdot \boldsymbol{\nu} = \sum_E \int_E \hat{\psi}_E \nabla \cdot \boldsymbol{\nu} \, d\mathbf{x} = \sum_E \sum_{f \in F(E)} \hat{\psi}_E \int_f \boldsymbol{\nu} \cdot \mathbf{n} \, d\mathbf{x},$$

where $F(E)$ denotes the set of faces that belong to E . The last integral can be computed exactly as shown in (25). We have

$$(36) \quad \int_{\Omega} \hat{\psi} \nabla \cdot \phi_{\eta,k} \, d\mathbf{x} = \sum_{j \in E(\eta)} \sum_{f_{j,l} \in E_j \cap E_l} \hat{\psi}_{E_j}(\mathbf{e}_k \cdot \mathbf{n}_{j,l}) \int_{f_{j,l}} \phi_l \, d\mathbf{x},$$

with the convention that we only get contribution in the integral when the face $f_{i,j}$ exists, that is when E_j and E_l share a common face. Note that by definition of the exterior normal, we have $\mathbf{n}_{j,l} = -\mathbf{n}_{l,j}$. We use (25) to compute the integral and therefore the divergence operator $\text{div} : \mathcal{T} \rightarrow \mathcal{V}$ is defined. The transpose of the discrete divergence operator will give us an approximation of a discrete gradient. We can obtain an expression of the discrete gradient by reverting the order of the sum in (36). Let us denote by $F(\eta)$ the set of faces the node η belongs to and, for a face f_k , we denote the neighboring cells of f_k by E_k^+ and E_k^- . From (36), we can rewrite

$$\int_{\Omega} \hat{\psi} \nabla \cdot \phi_{\eta,k} \, d\mathbf{x} = - \sum_{f_k \in F(\eta)} (\hat{\psi}_{E_k^+} - \hat{\psi}_{E_k^-})(\mathbf{e}_k \cdot \mathbf{n}_l) \int_{f_l} \phi_l \, d\mathbf{x}.$$

where the normal \mathbf{n}_k of the face f_k is directed from E_k^- to E_k^+ . This convention implies that $\mathbf{n}_{jl} = -\mathbf{n}_{lj} = \mathbf{n}_k$ if $E_j = E_k^-$ and $E_l = E_k^+$. Hence, the discrete gradient operator grad is the mapping from scalar cell values to vector node value given by

$$(37) \quad [\text{grad}(\hat{\psi})]_{\eta,k} = \sum_{f_k \in F(\eta)} (\hat{\psi}_{E_k^+} - \hat{\psi}_{E_k^-})(\mathbf{e}_k \cdot \mathbf{n}_l) \int_{f_l} \phi_l \, d\mathbf{x}.$$

Hence, gathering (34), (35) and (37), in this formulation, we obtain the following expression for $\hat{\mathbf{f}}$, as the discrete gradient of the discretized potential, that is

$$\hat{\mathbf{f}} = \text{grad}(\hat{\psi}).$$

We note that (37) only depends on the local difference in the potential, which can be estimated locally without knowledge of the global potential, i.e $\hat{\psi}_{E_k^+} - \hat{\psi}_{E_k^-} = \mathbf{f}_k \cdot \mathbf{d}\mathbf{r}$, where $\mathbf{d}\mathbf{r}$ is the vector between the centroids of E_k^{\pm} .

In [7], the stabilization term in (28) is given as

$$(38) \quad \mathbf{S} = \alpha \mathbf{I}$$

where the constant α is chosen as

$$(39) \quad \alpha_G = \frac{|E| \text{tr}(\hat{\mathbf{C}})}{\text{tr}(\mathbf{N}_c^T \mathbf{N}_c)}$$

This constant is stable with respect to isotropic scaling but not with respect to aspect ratio. To demonstrate that, we consider a rectangular element in 2D given by $[-h_1, h_1] \times [-h_2, h_2]$. In this case, we have explicit expressions for the virtual basis elements, which are given by

$$(40) \quad \varphi_1^l(\mathbf{x}) = 1, \quad \varphi_2^l(\mathbf{x}) = \frac{x_1}{h_1}, \quad \varphi_3^l(\mathbf{x}) = \frac{x_2}{h_2}, \quad \varphi(\mathbf{x}) = \frac{x_1 x_2}{h_1 h_2},$$

in each Cartesian direction. They correspond in fact to the standard finite elements. The functions $\varphi_j^l(\mathbf{x})\mathbf{e}_i$ for $j = 1, 2, 3$ and $i = 1, 2$ provides a basis for the affine space \mathcal{P} . Let $\varphi_i(\mathbf{x}) = \varphi(\mathbf{x})\mathbf{e}_i$. We check directly, using the symmetry of the domain, that

$$\boldsymbol{\pi}^{\nabla}(\varphi_i) = 0.$$

Hence, for each basis functions in (40), we have that the zero and first order moments correspond to those of their projection so that, indeed, they form a basis of \mathcal{V} . Moreover $\{\varphi_i\}_{i=1,2}$ constitutes a basis for $\ker \boldsymbol{\pi}^\nabla$. In this two-dimensional case, the matrix \mathbf{N}_c is given by

$$\mathbf{N}_c^i = \begin{pmatrix} h_1 & 0 & \frac{1}{\sqrt{2}}h_2 \\ 0 & h_2 & \frac{1}{\sqrt{2}}h_1 \end{pmatrix}$$

We collect the contributions of the four nodes of the cell and obtain the matrix \mathbf{N}_c given by

$$(41) \quad \mathbf{N}_c^T = \begin{pmatrix} h_1 & 0 & -h_1 & 0 & -h_1 & 0 & h_1 & 0 \\ 0 & h_2 & 0 & h_2 & 0 & -h_2 & 0 & -h_2 \\ \frac{1}{\sqrt{2}}h_2 & \frac{1}{\sqrt{2}}h_1 & \frac{1}{\sqrt{2}}h_2 & -\frac{1}{\sqrt{2}}h_1 & -\frac{1}{\sqrt{2}}h_2 & -\frac{1}{\sqrt{2}}h_1 & -\frac{1}{\sqrt{2}}h_2 & \frac{1}{\sqrt{2}}h_1 \end{pmatrix}$$

which yields

$$(42) \quad \mathbf{N}_c^T \mathbf{N}_c = \begin{pmatrix} 4h_1^2 & 0 & 0 \\ 0 & 4h_2^2 & 0 \\ 0 & 0 & 2(h_1^2 + h_2^2) \end{pmatrix}$$

so that $\text{tr}(\mathbf{N}_c^T \mathbf{N}_c) = 6(h_1^2 + h_2^2)$. Hence, the scaling ratio α_G is given by

$$(43) \quad \alpha_G = \frac{4h_1 h_2 \text{tr}(\hat{\mathbf{C}})}{6(h_1^2 + h_2^2)} = \frac{2}{3} \frac{\text{tr}(\hat{\mathbf{C}})}{(\varepsilon + \varepsilon^{-1})},$$

where $\varepsilon = \frac{h_1}{h_2}$ denotes the aspect ratio. Let us now compute how this weight in the stabilization term compares with the actual energy for the functions that belong to $\ker \boldsymbol{\pi}^\nabla$. To do so, we consider an isotropic material where the stress is given as

$$(44) \quad \boldsymbol{\sigma} = \lambda \text{tr}(\boldsymbol{\varepsilon}) + 2\mu \boldsymbol{\varepsilon},$$

which implies

$$(45) \quad a(\mathbf{u}, \bar{\mathbf{u}}) = \int_{\Omega} (\lambda \text{tr}(\boldsymbol{\varepsilon}) \text{tr}(\bar{\boldsymbol{\varepsilon}}) + 2\mu \boldsymbol{\varepsilon} : \bar{\boldsymbol{\varepsilon}}) \, d\mathbf{x}$$

For φ_i we denote by $\boldsymbol{\varepsilon}_i$, the corresponding strain, which is given by

$$(46) \quad \boldsymbol{\varepsilon}_i = \frac{1}{2} (\mathbf{e}_i \nabla \phi^T + \nabla \phi \mathbf{e}_i^T).$$

We get

$$\boldsymbol{\varepsilon}_i : \boldsymbol{\varepsilon}_j = \frac{1}{2} \left(\delta_{i,j} |\nabla \varphi|^2 + \frac{\partial \varphi}{\partial x_i} \frac{\partial \varphi}{\partial x_j} \right),$$

where $\delta_{i,j} = 1$ if $i = j$ and zero otherwise. Hence, using the symmetry of the domain, we get

$$\int_E \boldsymbol{\varepsilon}_i : \boldsymbol{\varepsilon}_j \, d\mathbf{x} = \delta_{i,j} \int_E |\nabla \varphi|^2 \, d\mathbf{x}.$$

We have $\text{tr}(\boldsymbol{\varepsilon}_i) = \frac{\partial \varphi}{\partial x_i}$. Hence, using the symmetry of the domain we get

$$\int_E \text{tr}(\boldsymbol{\varepsilon}_i) \text{tr}(\boldsymbol{\varepsilon}_j) \, d\mathbf{x} = \delta_{i,j} \int_E \left| \frac{\partial \varphi}{\partial x_i} \right|^2 \, d\mathbf{x}.$$

Finally, the restriction of the bilinear form a to $\ker \pi^\nabla$ takes the form

$$a(\varphi_i, \varphi_j) = \begin{pmatrix} \int_E \left(\lambda \left| \frac{\partial \varphi}{\partial x_1} \right|^2 + 2\mu |\nabla \varphi|^2 \right) dx & 0 \\ 0 & \int_E \left(\lambda \left| \frac{\partial \varphi}{\partial x_2} \right|^2 + 2\mu |\nabla \varphi|^2 \right) dx \end{pmatrix}$$

The integrals above can be computed exactly and we have

$$\int_E \left| \frac{\partial \varphi}{\partial x_1} \right|^2 dx = \frac{4}{3} \varepsilon^{-1}, \quad \int_E \left| \frac{\partial \varphi}{\partial x_2} \right|^2 dx = \frac{4}{3} \varepsilon,$$

Hence,

$$a(\varphi_i, \varphi_j) = \begin{pmatrix} \frac{4}{3} \lambda \varepsilon^{-1} + \frac{8}{3} \mu (\varepsilon + \varepsilon^{-1}) & 0 \\ 0 & \frac{4}{3} \lambda \varepsilon + \frac{8}{3} \mu (\varepsilon + \varepsilon^{-1}) \end{pmatrix}.$$

We denote by α_1 and α_2 the two eigenvalues of the matrix above. We obtain

$$\lim_{\varepsilon \rightarrow 0, \infty} \frac{\alpha_1}{\alpha_G} = \lim_{\varepsilon \rightarrow 0, \infty} \frac{\alpha_2}{\alpha_G} = \infty$$

This enables us to conclude that, when the aspect ratio ε tends either to zero or infinity, the ratios above tends to infinity so that we cannot find a constant $c > 0$, independent of the aspect ratio ε , such that

$$ca_E(\mathbf{u}, \mathbf{u}) \leq s_E(\mathbf{u}, \mathbf{u}),$$

for all $\mathbf{u} \in \ker \pi^\nabla$. It implies that the stabilization term is not stable with respect to the aspect ratio. Instead of using α_G , let us use

$$\alpha_N = \frac{1}{9} |E| \operatorname{tr}(\hat{\mathbf{C}}) \operatorname{tr}(\operatorname{inv}(\mathbf{N}_c^T \mathbf{N}_c)).$$

Both α_N and α_G are invariant with respect to rotation. Because of the coefficient $\frac{1}{9}$, we have that if $\mathbf{N}_c^T \mathbf{N}_c$ were diagonal with constant coefficient, then α_N and α_G would be equal. But in general they differ and we have

$$(47) \quad \alpha_N = \frac{2\lambda + 6\mu}{4} \left(\varepsilon + \varepsilon^{-1} + \frac{2}{\varepsilon + \varepsilon^{-1}} \right)$$

It implies that

$$\lim_{\varepsilon \rightarrow 0} \frac{\alpha_1}{\alpha_N} = \lim_{\varepsilon \rightarrow \infty} \frac{\alpha_2}{\alpha_N} = \frac{16}{3} \frac{\lambda + 2\mu}{\lambda + 3\mu}$$

and

$$\lim_{\varepsilon \rightarrow \infty} \frac{\alpha_1}{\alpha_N} = \lim_{\varepsilon \rightarrow 0} \frac{\alpha_2}{\alpha_N} = \frac{16}{3} \frac{\mu}{\lambda + 3\mu}.$$

Therefore, for this choice of α , there exist two constants $c_1, c_2 > 0$ which are *independent* of the aspect ration ε and such that

$$c_1 a_E(\mathbf{u}, \mathbf{u}) \leq s_E(\mathbf{u}, \mathbf{u}) \leq c_2 a_E(\mathbf{u}, \mathbf{u})$$

for all $\mathbf{u} \in \ker \pi^\nabla$. We can conclude that the regularization provided by α_N is stable with respect to the aspect ratio.

4. NUMERICAL TEST CASES

The great advantage of VEM methods is that they are valid for very general grids including non-convex cells and more than one face between two cells, [3]. This property can be used to avoid curved faces on general cells, simply by triangulating the surface. The VEM theory does not cover curved surfaces and in the next examples we investigate the need for triangulation in 3D.

4.1. Compaction 2D. To evaluate the effects of the different computation methods of the force term, we consider a Cartesian grid which we twist in order to avoid artifact effects from symmetries. The force we consider is gravity. In this case, the projection method as described is exact. Indeed we have, for any $\mathbf{u} \in \mathcal{V}$,

$$\int_{\Omega} \mathbf{f} \cdot \mathbf{u} \, d\mathbf{x} = \int_{\Omega} \rho g \mathbf{e}_z \cdot \mathbf{u} \, d\mathbf{x} = \rho g \mathbf{e}_z \cdot \int_{\Omega} \mathbf{u} \, d\mathbf{x} = \rho g \mathbf{e}_z \cdot \int_{\Omega} \boldsymbol{\pi} \nabla \mathbf{u} \, d\mathbf{x},$$

and the last integral can be computed exactly from the degree of freedom. Hereafter, we will therefore refer to this method for computing the load term as the *exact* method. We use $\rho = 3 \times 10^3 \text{ kg m}^{-3}$, $E = 3 \times 10^8 \text{ Pa}$ and $\nu = 0.3$. We impose zero displacement in the third direction. The vertical size of the grid is 15m. We compare the behavior of the different methods for computing the load term as the aspect ratio is increased. In addition to the twisted Cartesian grid, we consider also a the grid which is obtained by adding an extra node on the vertical faces, see figure 1.

The most pronounced effect we observe is the severe dependence on the aspect ratio for the exact integration, as it can clearly be seen in the upper right corner of the panels of Figure 1. For the dual approach there is no noticeable effect. Figure 2 shows the dependence of $err(d_z)/max(d_z)$ for the different grids and force calculations. The left figure shows that for the the exact force calculation fail for the grid with extra nodes. We also observe that the error follows a second order scaling with aspect ratio, $err \sim (L_y/L_x)^2$. The right figure show the error for the projected force for the Cartesian grid and dual approach for the Cartesian grid and the grid with extra nodes. All the methods give reasonable results, but the projection calculation seems to deteriorate more than the others. The dual approach is stable in both cases. If we had used a grid without disturbance all the methods would give exact results for the grid without extra nodes on the faces while the extra node case will still fail for the projected force calculation. As explained in the previous section, see (30), the difference between the methods is in how the they divide the weights between the nodes. All the force-based methods divide forces according to a weight for each node associated with volume integrals. These weights will be equal for all direction. The dual method uses weights associated with surface integrals. In this case the weights can depend on the direction, i.e degree of freedom. These weights can be associated with the projected area of the faces associated with a node divided by the projection of the cell in the same direction. In the case of the extra nodes this nodes will have associated weights in the horizontal direction only due to the tilt of the grid and the weights will in the simple case be doubled of the corner nodes while the exact case will give all nodes the same weights. In [7] a third method which uses node quadrature was considered, this will in the above case give a smaller weight to the midpoint and behave worse for the case with extra node, as seen in the left panel of Figure 2. Finally in Figure 3, we consider the new scaling α_N , which is stable with respect to aspect ratio. As expected, the error does not grow as the aspect ratio is increased. The use of α_N deteriorates the solution computed using the dual approach while it significantly improves the solution using the exact method. However, this conclusion is difficult to extend to more general cases. The value α_N has been derived from an analysis done on regular quadrilaterals and we observe that the stability properties extend to a twisted Cartesian grid. However, separate studies would have to be done for more complicated shapes and also in 3D. While in 2D the aspect ratio is described

by a scalar quantity namely $\varepsilon = \frac{\Delta x}{\Delta y}$, in 3D we need 2 values, say $\frac{\Delta x}{\Delta z}$ and $\frac{\Delta y}{\Delta z}$, the third quantity $\frac{\Delta x}{\Delta y}$ being imposed by the fact that we will anyway require isotropic stability. It means that a scalar approximation of the regularization term, as given in (38) and also in [5], will not be enough. This problem was noticed in , and the exact regularization term corresponding to finite element was used to study poro-elastic response function in 3D case, we refer to [2].

Twisted Cartesian grid

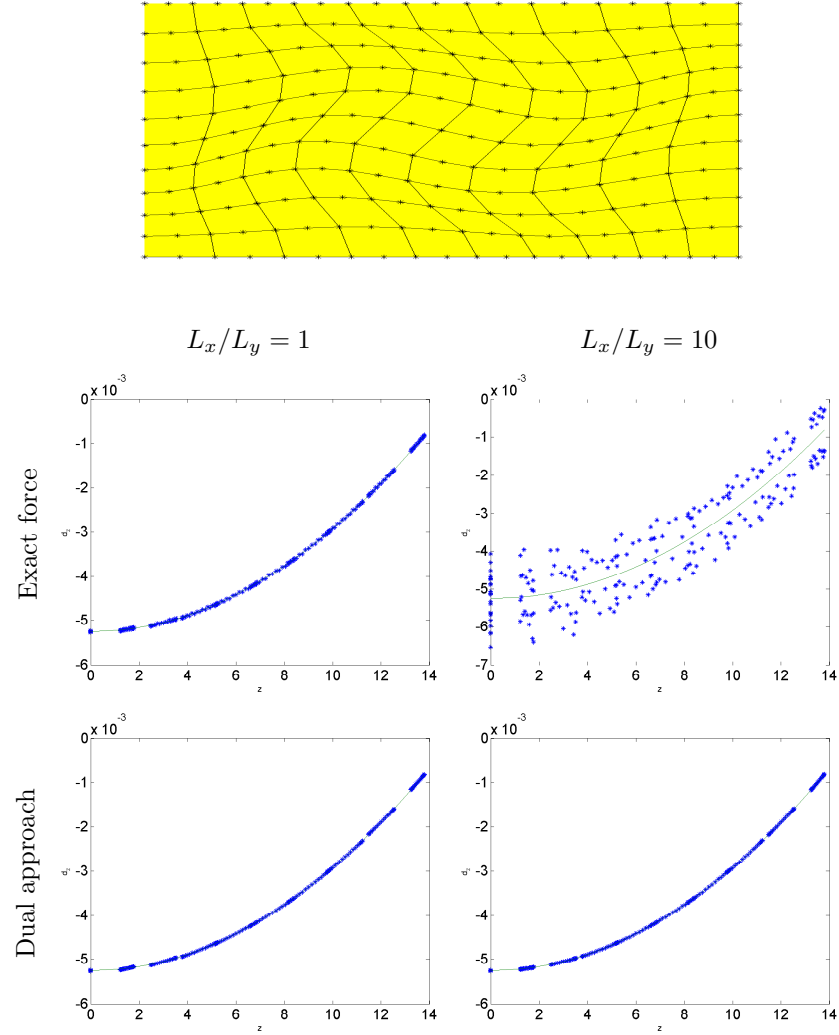


FIGURE 1. Comparing the calculated displacement in vertical direction for a grid with extra node at all vertical faces as shown in top pannel. The left column is for aspect ratio 1 and the right is for aspect ratio 10. The first row is using force calculation based on the exact integration of the VEM basis function [7], while the lower row is using the dual div based method.

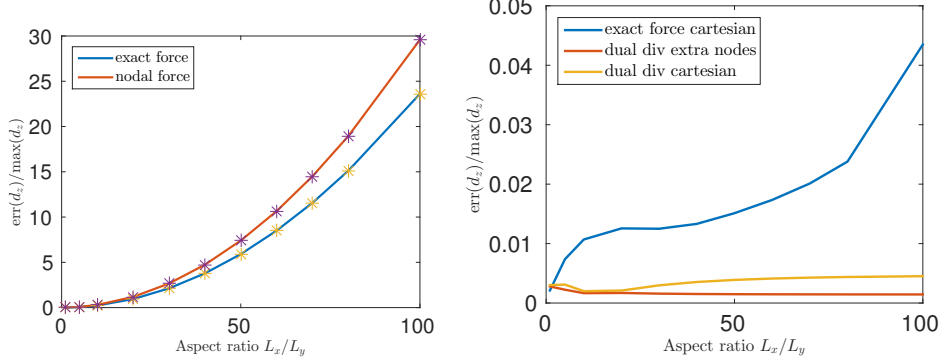


FIGURE 2. The error of the vertical displacement as for different aspect ratios. The left figure shows the exact integration method for the case with extra nodes on vertical faces, which fails. The points in a the figure is correspond to a simple second order scaling of the error with aspect ratio. The right the same for exact with Catesian grid and dual div based for Catesian and for the grid with extra nodes.

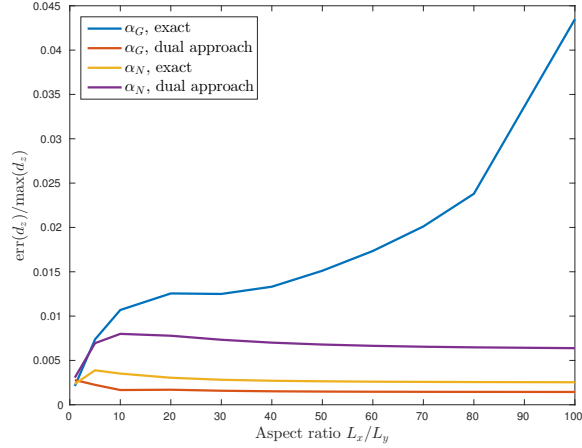


FIGURE 3. Comparison between the two regularization constants α_G and α_N . We plot the error of the vertical displacement, as the aspect ratios is increased. We observe that the stability constant α_N yields stability with respect to aspect ratio.

4.2. Compaction 3D. In order to investigate the performance of the VEM method on real reservoir geometries, we use two grids which includes standard features of subsurface models. The first one is based on a local sedimentary model called *sbed*. The model was used for upscaling permeability. Our version is $15m \times 15 \times 3m$ with logical Cartesian dimensions $15 \times 15 \times 333$. The grid reflects two of the basic properties of a sedimentary process, which are the layering and erosion processes. For this type of grid, the challenge is the degenerate cells and the large aspect ratios. The second model that we consider is taken from the open reservoir model of Norne. The data for this model is open and can be found in the open dataset of [12]. We extract a part of this model, pad it on all sides to embed it in a regular prism, so that we can directly compare the solution with the analytic solution of a pure gravitational compression. The final full model and the embedded model with faults are shown in Figure 6.

Both models use a corner-point grids, which is a standard in the industry. A corner-point grid has an underlying two dimensional structure which is used to index the pillars. The pillars are one dimensional lines, with a dominant vertical direction, to which nodes are attached. The cell edges are then created by joining adjacent nodes from the same pillar (vertical edges) or joining nodes of adjacent pillars (horizontal edges), see [13] or [9]. The construction naturally leads to faces that are not planar and set us outside the theoretical framework of the VEM method, which handle polygonal faces. However, the computation of the stiffness matrix for VEM relies on geometrical properties that are all available, either as exact or approximated values, in the case of a corner-point grid, so that the stiffness matrix can be assembled and a solution computed. To evaluate the error that is introduced by this geometrical approximation, we compare the solution obtained this way with the solution that is obtained after triangulating the non planar surfaces, by adding a point in the middle of the faces. For such grid, the faces will be planar and the theoretical framework of the VEM method applies.

In Figure 4, we show the effect of compression with two types of load given by a constant gravitational force and a constant force applied on the top surface. For both loads, the analytical solutions can be computed and they are respectively, quadratic and linear in z . We consider both the original corner-point grid and the triangulated grid. By triangulated grid, we mean a grid where the faces are triangulated, as we just explained. For all these cases, the VEM method gives accurate results, given that we use the dual approach to compute the load term. The other alternative simply fail in this case, by given errors that are larger than the span of the exact solution. In the *sbed* model, the pillars are all vertical lines, which implies that the vertical faces are planar. For the linear case corresponding a constant load on the top surface, we see that the triangulated version give exact result, as predicted by the VEM theory, since in this case all the surfaces are planar and the solution is linear. For the original grid, we get an error due to the curved top and bottom faces in each cell. For the pure gravitational case, both grids give comparable results. Thus, we can conclude that in practice, it may not be worth triangulating the faces as it introduces more degrees of freedom without significantly improving the accuracy of the solution. We consider the case of the flipped model in Figure 5. In this way, we can investigate the effect of having non planar surface in the vertical direction. Typically, for the cells of the original reservoir, we have $\frac{\Delta x}{\Delta z} \approx \frac{\Delta y}{\Delta z} \gg 1$ so that, by flipping the model, we can observe the

consequence of inverting the correlation between the aspect ratio and the direction of gravitation. The results are similar. However the triangulated case which is exact for linear compression highlights that the error of different types of nodes have different errors, see explanation in the caption of Figure 5.

Besides features like layering and erosion, the Norne case introduces also fault structures. Such grids are far from ideal for numerical calculation, but the VEM method shows very robust behavior. In Figure 6, we look at the difference between the original model and a model where all the pillars are straightened up and made vertical. In this way, the curved sides in the vertical direction are eliminated. The analytical solution is unchanged as we recall that the whole Norne model is anyway embedded in a regular prism. The results on Norne confirm those obtained for the *sbed* model and show that effects of curvature on the faces can be neglected. This indicates that, for many practical applications, the VEM method can be used directly on the original grid of reservoirs without deteriorating the accuracy of the results.

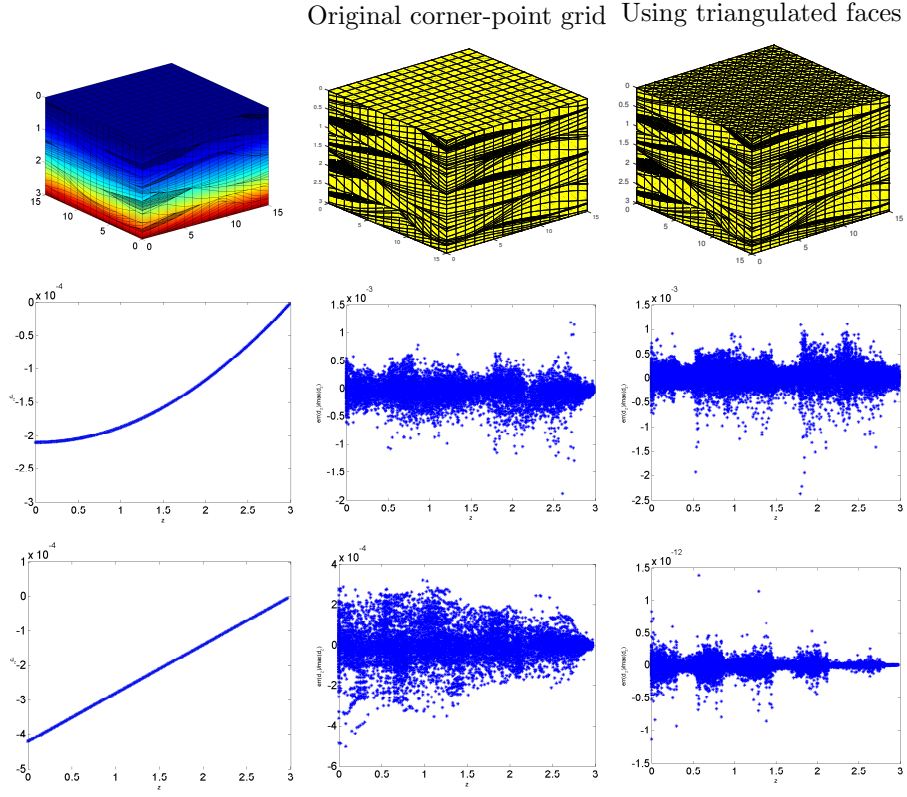


FIGURE 4. Effect of compression on the *sbed* model. The first row shows a plot of the vertical deformation on the grid (left), the original grid (middle) and the same grid where the surface are triangulated (right). Two types of loads are considered: pure gravitational compression (second row), load at the top surface (third row). The first column shows the displacement obtained for each loading case, which is very close to the analytical solution. The remaining plots show the errors for the original cornerpoint grid with curved faces (middle column) and the triangulated grid with only planar faces (right column).

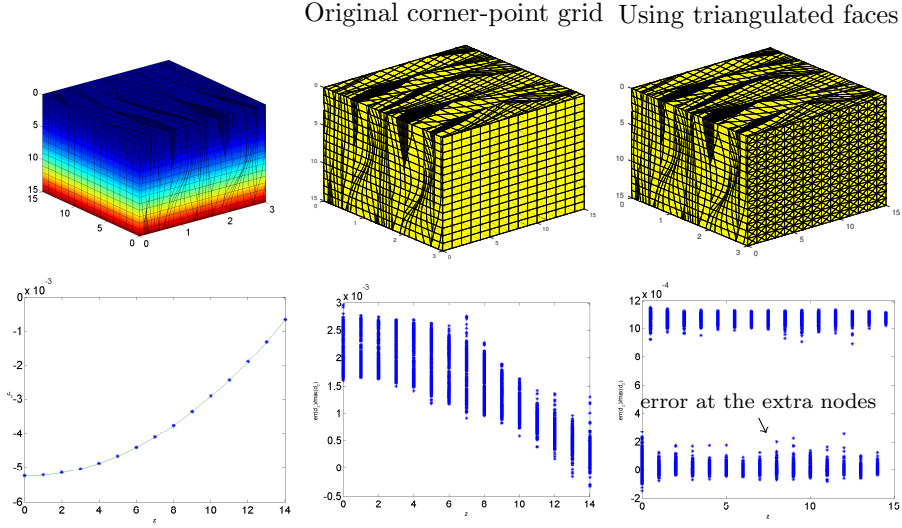


FIGURE 5. Effect of compression on a fliped *sbed* model. The first row shows a plot of the vertical deformation on the grid (left), the original grid (middle) and the same grid where the surface are triangulated (right). We consider only the case with gravitation load. The first column shows the displacement. The remaining plots show the errors for the original corner-point grid (middle column) and the triangulated grid (right column). On the plot at the lower right, we observe that the error splits clearly between the type of nodes, the extra face node at the bottom and the other at the top.

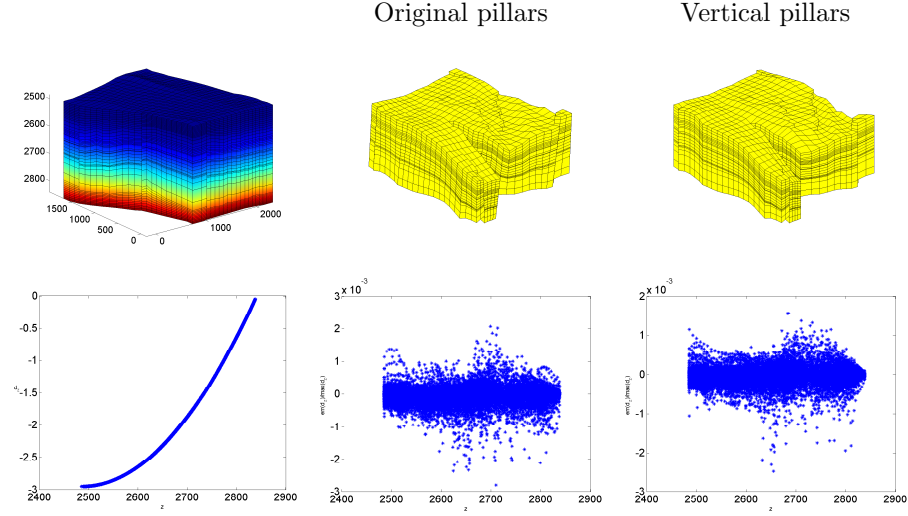


FIGURE 6. Effect of compression on a part of the Norne model. The first column shows the plot the vertical deformation on the grid (left), the original grid after removing the padding (middle) and the straightened grid where the pillars are made vertical (right). The figure in the upper left corner shows the bounding box which is used for the calculation, while the two other grids show the embedded Norne grid. The second row show the results for pure gravitational compression. The first column shows the vertical displacement while the second and third show the errors in the vertical displacement for the original and triangulated grid.

5. CONCLUSION

We have demonstrated how geomechanical calculations can be done directly on complex geological models frequently encountered in reservoir modeling. This was facilitated by the flexibility of VEM framework, which is due to the use of a virtual basis which can be defined on general geometries, the mechanical energy is only approximated. As we demonstrate, this approximation can come with the cost of large errors for deformed grids, if not care is taken when defining the approximate bilinear form. In particular we study the effect of the force calculation and showed that with a the regularization term and force calculation presented in the literature, even the simple case fails severely for the given reservoir grid (even if the method is convergent). We found that the problem is associated with a combination of the discretization and the force calculation. Based on the exact equivalence with FEM on quadrilateral we presented a modification of the discretization that makes the method more robust in the 2D case. In addition, we demonstrated that a calculation of the force in term of a gradient of a potential was robust in 2D and the only approach which gave sufficient accuracy in 3D. In particular, for grid cells which are outside the reach of FEM such as those containing for hanging nodes. The VEM theory does not cover curved faces which is often part of subsurface models. We saw that for our tests the error associated with this feature was negligible comparable with other errors, with the natural exception of the case when VEM gives the exact solution (linear displacement).

REFERENCES

- [1] B Ahmad, Ahmed Alsaedi, Franco Brezzi, L Donatella Marini, and A Russo. Equivalent projectors for virtual element methods. *Computers & Mathematics with Applications*, 66(3):376–391, 2013.
- [2] Odd Andersen, Halvor Møll Nilsen, and Sarah Gasda. Modelling geomechanical impact of CO_2 injection using precomputed response functions. In *ECMOR XV – 15th European Conference on the Mathematics of Oil Recovery, Amsterdam, Netherlands, 29 August - 1 September 2016*. EAGE, 2015.
- [3] L Beirão da Veiga, F Brezzi, A Cangiani, G Manzini, LD Marini, and A Russo. Basic principles of virtual element methods. *Mathematical Models and Methods in Applied Sciences*, 23(01):199–214, 2013.
- [4] P. G. Bergan and M. K. Nygård. Finite elements with increased freedom in choosing shape functions. *Int. J. Numer. Meth. Engng.*, 20(4):643–663, Apr 1984.
- [5] L Beirão Da Veiga, Franco Brezzi, and L Donatella Marini. Virtual elements for linear elasticity problems. *SIAM Journal on Numerical Analysis*, 51(2):794–812, 2013.
- [6] Lourenço Beirão da Veiga, Konstantin Lipnikov, and Gianmarco Manzini. *Mimetic Finite Difference Method for Elliptic Problems*, volume 11. Springer, 2014.
- [7] Arun L Gain, Cameron Talischi, and Glaucio H Paulino. On the virtual element method for three-dimensional linear elasticity problems on arbitrary polyhedral meshes. *Computer Methods in Applied Mechanics and Engineering*, 282:132–160, 2014.
- [8] Emmanuel J. Gringarten, Guven Burc Arpat, Mohamed Aymen Haouesse, Anne Dutranois, Laurent Deny, Stanislas Jayr, Anne-Laure Tertois, Jean-Laurent Mallet, Andrea Bernal, and Long X. Nghiêm. New grids for robust reservoir modeling. *SPE Annual Technical Conference and Exhibition*, 2008.
- [9] Knut-Andreas Lie. An introduction to reservoir simulation using matlab: User guide for the matlab reservoir simulation toolbox (mrst), 2015. SINTEF ICT.
- [10] KnutAndreas Lie, Stein Krogstad, Ingeborg Skjelkvåle Ligaarden, Jostein Roald Natvig, Halvor Nilsen, and Bård Skaflestad. Open-source MATLAB implementation of consistent discretisations on complex grids. *Comput. Geosci.*, 16:297–322, 2012.

- [11] Bradley Mallison, Charles Sword, Thomas Viard, William Milliken, and Amy Cheng. Unstructured cut-cell grids for modeling complex reservoirs. *SPE Journal*, 19(02):340352, Apr 2014.
- [12] Open Porous Media initiative. Open datasets, 2015. <http://www.opm-project.org>.
- [13] David K Ponting. Corner point geometry in reservoir simulation. In *ECMOR I-1st European Conference on the Mathematics of Oil Recovery*, 1989.